Thermochimica Acta 677 (2019) 12–20

Contents lists available at ScienceDirect

Thermochimica Acta

journal homepage: www.elsevier.com/locate/tca

Measurement of specific heat capacity via fast scanning calorimetry—Accuracy and loss corrections

C.R. Quick[a], J.E.K. Schawe[b], P.J. Uggowitzer[a], S. Pogatscher[a,*]

[a] Chair of Nonferrous Metallurgy, Department of Metallurgy, Montanuniversitaet Leoben, Franz-Josef-Str. 18, 8700 Leoben, Austria
[b] Mettler-Toledo GmbH, Heuwinkelstrasse 3, 8606 Nänikon, Switzerland

ARTICLE INFO

Keywords:
Fast scanning calorimetry
Chip calorimetry
Specific heat capacity
Metals

ABSTRACT

This study explores specific heat capacity (c_p) measurements via fast scanning calorimetry, with a focus on correcting measured heat flow by accounting for temperature dependent heat losses. Using MultiSTAR-UFS1 sensors with the Mettler-Toledo Flash-DSC 2+, c_p of Pb (99.998% purity) was measured in dependence of the sample mass and scanning rate. Masses from 0.3–5 µg were evaluated at rates of 100, 1000 and 2000 K s^{-1} in the temperature range −20 to 320 °C. Two correction methods are shown and compared to c_p results without corrections. Heat loss corrections are mandatory when measuring c_p, but are in particular important for low masses and rates. High consistency was found between the two proposed correction procedures giving good confidence in their viability. A slight but consistent overestimation of c_p compared to literature casts uncertainty upon the determined sample mass. Whilst the systems under study in this work encompass only pure Pb, the arguments and procedures of the shown method of c_p determination are applicable to any system in the absence of physical transformations.

1. Introduction

A non-adiabatic chip calorimeter based on a MEMS chip consisting of a heater and thermometer can be used for measurements in a wide heating and cooling rate range beyond the maximum scanning rate limit of conventional DSC. High heating rates can be achieved due to the low heat capacity of the measuring system. The non-adiabatic mode means that the sensor is surrounded by cold gas. This enables a fast heat reduction of the sensor and sample and consequently high cooling rates. This technique was developed by Christoph Schick in the last 20 years [1–5] and the technique is used for practically all kinds of metastable materials like polymers, metallic alloys, organic polymorphic substances, inorganic glass-formers, bio-based materials etc. An overview can be found in Ref. [7]. This paper is dedicated to Christoph Schick on the occasion of his 65th birthday.

Because of the small sample size in case of the fast scanning chip calorimetry, quantitative calorimetric measurements were not possible in the early time of this technique. The first problem was the determination of the sample size. For this the use of thermal effects has been recommended [8–11]. The first extensive investigations for quantitative determination of thermodynamic properties were performed by Cebe et al. [12–14] on polymer systems using the Flash DSC from Mettler-Toledo.

This technique is also used to study the metastable phase behavior in metallic alloys [15–22]. Particularly, the high heating rate makes it possible to study the thermodynamic properties of the metastable phases [23].

In this paper we study the accuracy and reproducibility of specific heat capacity measurements on the example of solid lead (Pb) via Fast Differential Scanning Calorimetry (FDSC) using the Mettler-Toledo Flash-DSC 2 +. Different possibilities of accounting for heat loss corrections and the influence of sample mass and applied rates are discussed.

2. Methods

2.1. FDSC measurements

Experiments were performed on the Mettler-Toledo Flash-DSC2+ using conditioned and temperature-corrected MultiSTAR UFS 1 sensors. The sensor support temperature of the FDSC was set at 233 K using a Huber intracooler TC100. The furnace was purged with Ar of 5 N purity at a flow rate of 60 ml min^{-1}.

For the Flash DSC 2+ the conditioning procedure has three tasks: The heating of the sensor to a certain temperature, a test for functionality and the determination of the electrical resistance of the heater.

* Corresponding author.
E-mail address: stefan.pogatscher@unileoben.ac.at (S. Pogatscher).

https://doi.org/10.1016/j.tca.2019.03.021
Received 21 January 2019; Received in revised form 11 March 2019; Accepted 15 March 2019

To do this the sensor support should be thermally equilibrated. This means the intracooler is switched off for at least 5 h and the gas (Ar) flows before the conditioning procedure is applied. The temperature correction procedure measures the voltage of the thermocouples with respect to the sensor support temperature, Tss. For this procedure Tss has to be the ready temperature (here 233 K) and the gas has to be Ar (for UFH 1 sensors) and Ar or N_2 (for UFS 1 sensors). After correction different gasses can be used.

For exploring the potential to determine c_p via FDSC, high purity Pb-foil (99.998%) was chosen as a test material. The enthalpy of melting was measured at 100 K s^{-1}, in the interval 25–400 °C, and repeated 11 times. The first of these measurements was always rejected, since it is the least consistent. The remaining curves were used to produce an average melting peak, the integration of which yielded the average enthalpy of melting, ΔH_m. Sample mass (m_{FDSC}) was calculated using the enthalpy of fusion of Pb ($\Delta H_{fus}^{Pb} = 4.81$ kJ mol^{-1}) and its molar mass ($A_r^{Pb} = 207.2$ g mol^{-1}) from Smithell's Metals Reference Book [6], according to Eq. (1).

$$m_{FDSC} = \Delta H_m \times \frac{A_r^{Pb}}{\Delta H_{fus}^{Pb}} \quad (1)$$

FDSC samples were prepared by cutting a Pb-foil of 100 µm under a stereomicroscope to small pieces with weights of 0.3–5 µg. Table 1 depicts the exact weights and the used sensors.

For all experiments to determine the specific heat capacity the samples were heated or cooled between −20 °C and 320 °C. Samples underwent simple heating-cooling cycles with heating rates of 100, 1000 and 2000 K s^{-1}. Each heating-cooling rate was cycled 11 times, and the ten most consistent curves were implemented. Before conversion to c_p, the measurement curves were shifted in the temperature to adjust for the observed melting onset of the lead samples at 100 K s^{-1}, which is normally a minor temperature correction in the order of a few Kelvin.

2.2. Heat flow signal analysis

In the conventional DSC the heat capacity of the sample is significantly lower than the furnace. Consequently, the behavior of the furnace can be widely corrected from the measuring curve by subtraction of the blank curve measured without a sample [24]. In the case of FDSC measurements the situation is completely different. For the measurement of the bulk behavior of a gold based bulk metallic glass alloy the critical sample mass, at which the surface influence on the thermal behavior can be neglected, is in the order of 1 µg [10]. At such conditions the heat capacity of the sample is in the order of the heat capacity of the active zone of the FDSC sensor and consequently the empty sensor cannot be used as a blank curve. Due to the relatively large temperature difference between the hot sensor and the cold surrounding gas, the thermal losses between sample and reference side of the differential calorimeter cannot be completely compensated. Thus the measured heat flow can be described by

$$\Phi = m \bullet c_p \bullet \beta + \Phi_1 \quad (2)$$

Where m is sample mass, c_p is specific heat capacity of the sample, β is heating rate and Φ_1 is the heat loss function, which is in a good approximation independent of the scanning rate [8,12]. This relationship provides two straightforward ways to evaluate the heat loss function and thereby determine the actual heat flow into the sample, both of which are employed and compared in this work. The first method to find the heat loss function uses a low heating rate to minimize the sample term in Eq. (2), and thereby approximate the measured heat flow to the loss function (Eq. 3) [7].

$$\Phi_{\beta \to 0} = \Phi_1 \quad (3)$$

Since this method utilizes a low rate to determine the correction function, it is termed here the *slow-rate correction*. Note that the heat losses are not necessarily equal on heating and cooling, and so a separate slow-rate correction function is found for heating and cooling, and these are separately applied to the measured heating and cooling scans at higher rates.

Conversely, at high heating rate the contribution of the heat loss function to the measured heat flow will be relatively small, meaning the measured heat flow more closely resembles the sample heat flow.

The second method uses the average heat flow from heating and cooling to determine the heat loss function (Eqs. 4.1, 4.2), and is referred to as the *symmetry correction*.

$$\Phi_{avg} = \frac{(m \bullet c_p \bullet \beta + \Phi_{1,h}) + (m \bullet c_p \bullet (-\beta) + \Phi_{1,c})}{2} \quad (4.1)$$

$$\Phi_{avg} = \frac{\Phi_{1,h} + \Phi_{1,c}}{2} = \Phi_1 \quad (4.2)$$

where $\Phi_{1,h}$ and $\Phi_{1,c}$ are the heat loss functions for the heating and cooling measurement, respectively.

The calculated loss function can now be used to correct the heat flow, and the conversion to specific heat accomplished by dividing by the programmed heating rate and the sample mass (Eq. 5).

$$\frac{\Phi - \Phi_1}{m \bullet \beta} = c_p \quad (5)$$

The latter procedure was recommended by Zhuravlev and Schick [8].

3. Results

3.1. Measured curves and cp conversion without corrections

Shown in Fig. 1 are the measured heat flow curves from simple heating-cooling cycles at three different rates for four different masses. At each rate the heating-cooling segments were measured over 11 cycles, and the 10 most consistent curves are displayed and used in further calculations. "H100" denotes the measured heating cycles at 100 K s^{-1} and "C100" the cooling cycle measurements at 100 K s^{-1}. Similarly, those labelled 1000 and 2000 denote measurements at rates of 1000 and 2000 K s^{-1}. This convention is used throughout the figures to differentiate between the multitude curves. Good reproducibility is evinced by the consistency of the measured curves. The measured heat flow increases with increasing mass and rate (since more power is needed to achieve heating in those cases). Also worthy of note is the impact of the initial thermal stabilization on the measured heat flow, causing a perturbation at the beginning of the scanning run (at low temperatures for heating segments and at high temperatures for cooling segments). Due to the increased thermal lag this switching behavior of the heat flow becomes greatly exaggerated at higher masses and rates, and has a clear and noticeable impact on the range of useful results.

In Fig. 2, a single heat flow curve was taken from each of those measured above (1 heating and 1 cooling curve from each mass and rate) and converted to c_p, dividing by heating rate and sample mass. It is clear from Fig. 2 that measurements at 100 K s^{-1} show no correlation to literature data, and in all cases the sample of lowest mass, Pb0.3, has the poorest resemblance to the expected values. The samples of larger mass perform better at the elevated rates 1000 and 2000 K s^{-1},

Table 1
Sample name, exact weights and the used sensors.

Pb sample	Mass [µg]	UFS1 Sensor ID #
Pb0.3	0.286	XEN C17 42965
Pb1.3	1.26	XEN C17 42962
Pb2.6	2.56	XEN C17 42963
Pb5.3	5.26	XEN C17 42960

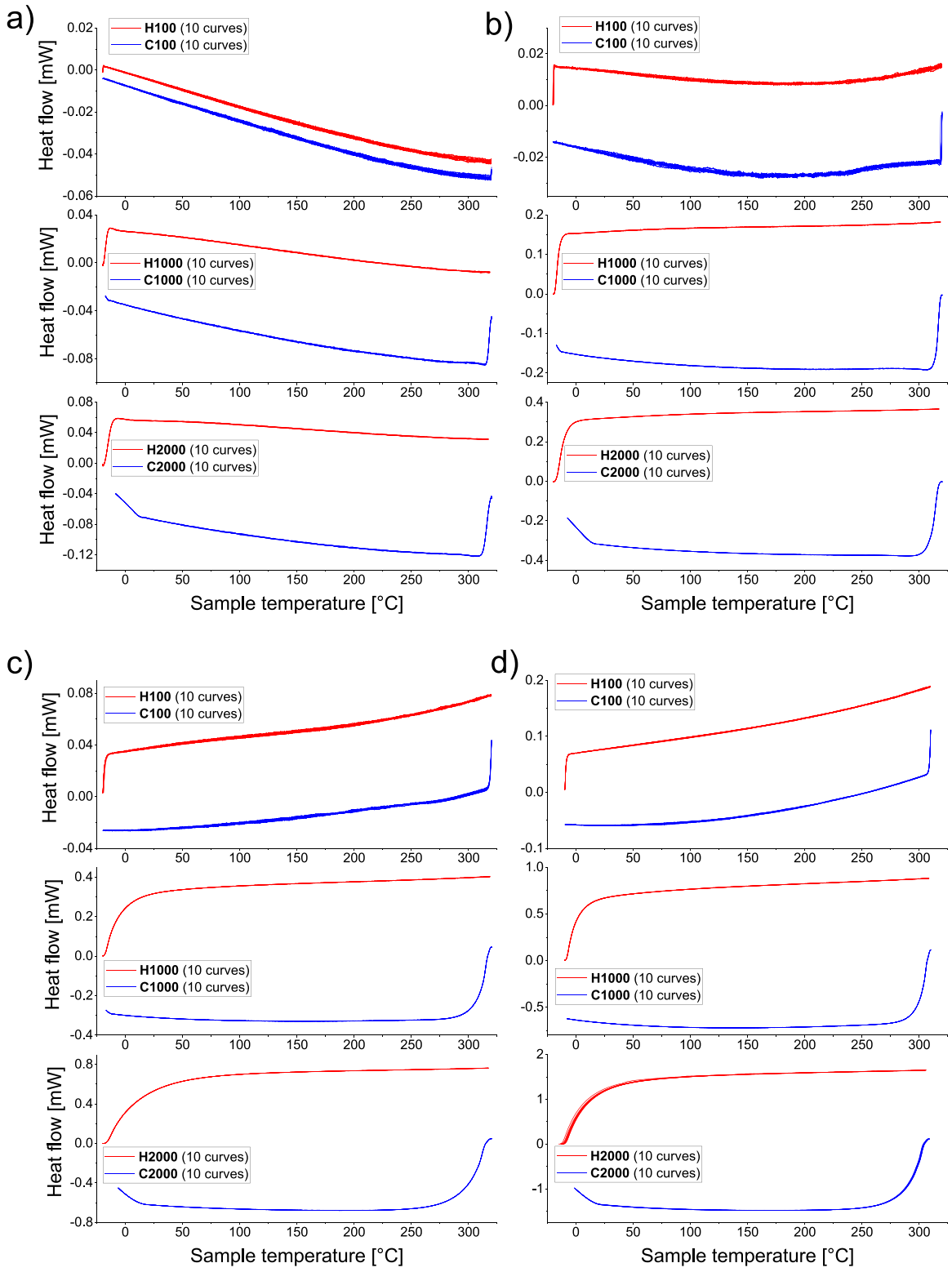

Fig. 1. Measured raw data heat flow curves for Pb masses Pb0.3 (a), Pb1.3 (b), Pb2.6 (c) and Pb5.3 (d) at linear heating and cooling rates of 100, 1000 and 2000 K s^{-1}. Ten curves are displayed at each rate to show reproducibility. At higher rates and masses, the levelling of the machine affects a wider temperature range. Endothermic signal is in the positive y-direction.

particularly on heating scans, though still fall short of usefully describing c_p. Interestingly, the H1000 curve for mass Pb1.3 in Fig. 2 (b) correlates very well with the literature prediction, however since this accuracy is not found in any other case the result is considered remarkable, but appears to be a result by chance. It is clearly shown then, that direct evaluation of the measured heat flow curves cannot determine the heat capacity without correction procedures.

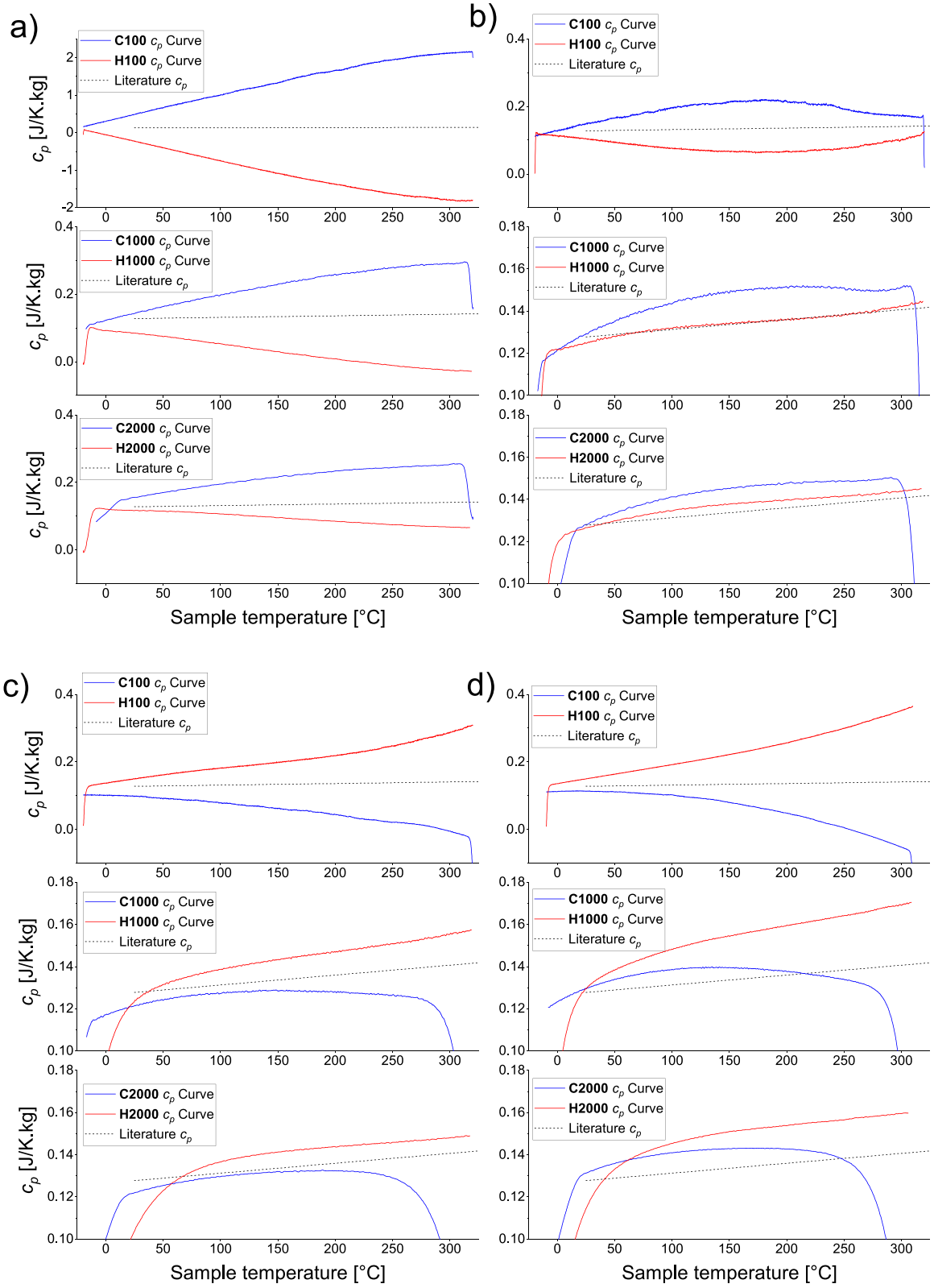

Fig. 2. Specific heat capacity curves calculated from raw data for samples Pb0.3 (a), Pb1.3 (b), Pb2.6 (c) and Pb5.3 (d), presented as in Fig. 1. A single sample curve from each linear heating and cooling rate was used in the conversion to specific heat capacity, and is compared to [6]. Low rate measurements show no correlation to literature expectation, and the smallest sample mass Pb0.3 is worst in all cases. The larger masses at higher rates fare better (note the smaller scales) though leave great room for improvement. The aforementioned stabilisation effects are also strongly visible here, clearly impacting the range of useful results.

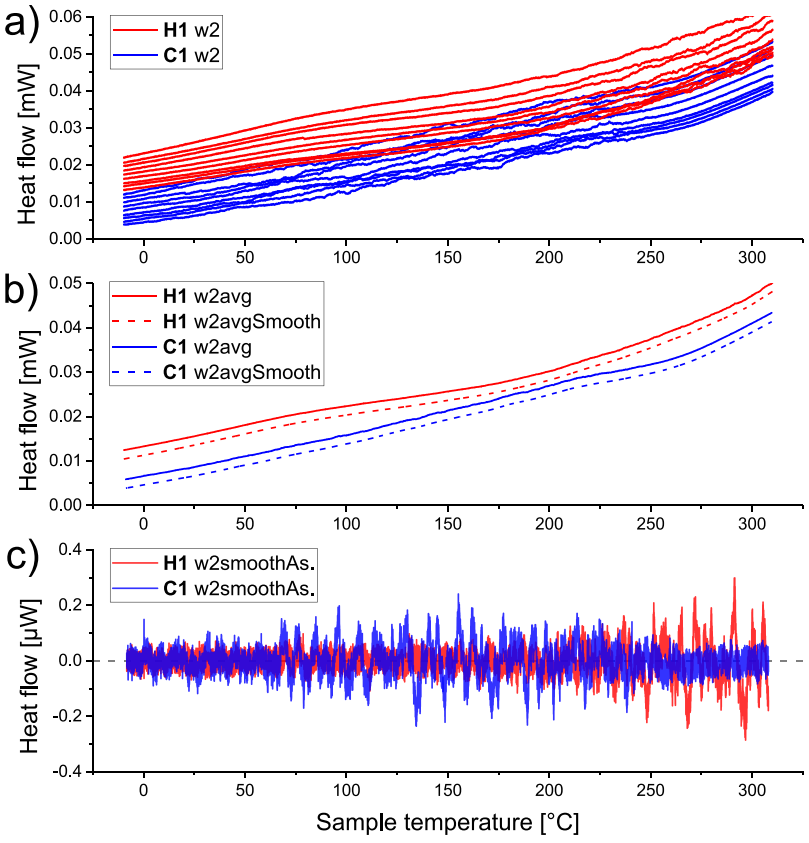

Fig. 3. Formation of the slow-rate loss correction curves for sample Pb2.6. (a) the measured curves at 1 K s^{-1}, (b) the average of the heating and cooling scans and their 1000-point smoothed counterparts, and (c) the smoothing assessed by subtraction of the smoothed curve from the unsmoothed average. Endothermic signal is in the positive y-direction.

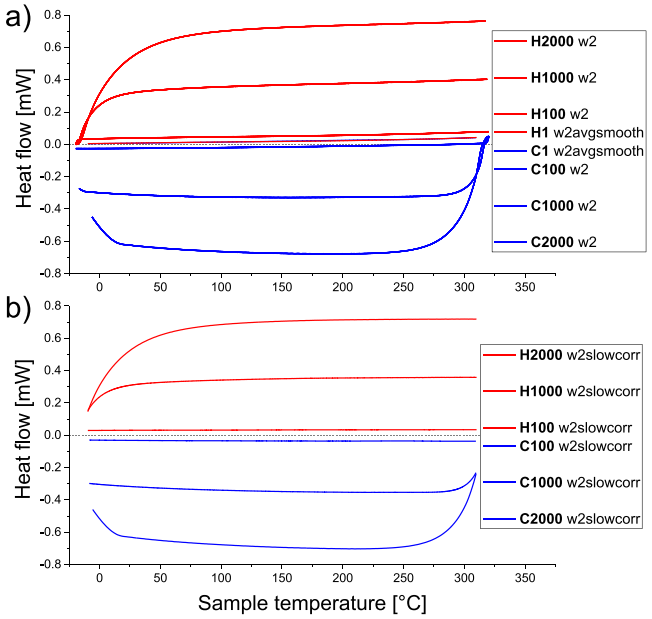

Fig. 4. Slow-rate correction applied to sample Pb2.6. (a) shows the 10 measured curves at individual rates before the subtraction of the slow-rate loss correction curve, and in (b) the slow-rate subtraction is performed to all individual curves and then the corrected curves are averaged at each respective rate. Endothermic signal is in the positive y-direction.

3.2. Procedure of heat loss corrections via slow-rate and symmetry approaches

According to Eqs. (2 and 3), the heat flow measured at sufficiently low rate can be approximated to only the heat losses. Since the slow-rate employed in this work (1 K s^{-1}) is two orders of magnitude lower than the slowest rate of interest, the sample effects are also 2 orders of magnitude lower and this is certainly sufficiently low to use such a curve as a base line. Figs. 3 and 4 show the implementation of the slow-rate correction method by producing the loss correction curves (Fig. 3) and subtracting them from the measured heat flow data (Fig. 4) for the relevant mass. First, heating and cooling scans at 1 K s^{-1} are separately averaged using the most consistent curves from the results. These are in fact already the loss correction curves, however before using them in any summation it is pertinent to remove signal noise by smoothing. To check that smoothing has not removed any real signal artefact, a smooth assessment is performed by subtracting the actual curves by their smoothed counterparts. The result shows what has been removed in the smoothing operation and should only be low intensity noise oscillations, which is indeed the result in Fig. 3(c) (note the µW scale). The smoothed averages produced are then subtracted from the sample's heat flow data at higher rates to produce the slow-rate heat loss corrected heat flow. The heating scans are subtracted by the heating slow-rate correction curve, and the cooling scans are subtracted by the cooling slow-rate correction curve.

Fig. 5 shows the production and implementation of the symmetry correction curves for sample Pb2.6 at the three rates of interest. Contrary to the slow-rate correction, the symmetry correction method uses a different correction curve for each rate measured. To produce the symmetry loss-correction curve (see Eq. 4.1) the total average of the heating and cooling scans at the same rate is found, displayed in green in the left part of Fig. 5 (a–c). This correction curve is then subtracted from the average heating and average cooling scans, separately. This yields the symmetry corrected heat flow (see right part of Fig. 5 (a–e)). Due to the averaged nature of the loss correction curve, the symmetry corrected heat flow for heating and cooling scans are in fact equal and opposite in magnitude. Since the heating and cooling rates are also equal and opposite in magnitude, conversion to c_p produces two identical curves. Therefore, only one of the curves is needed to calculate the symmetry corrected c_p curve.

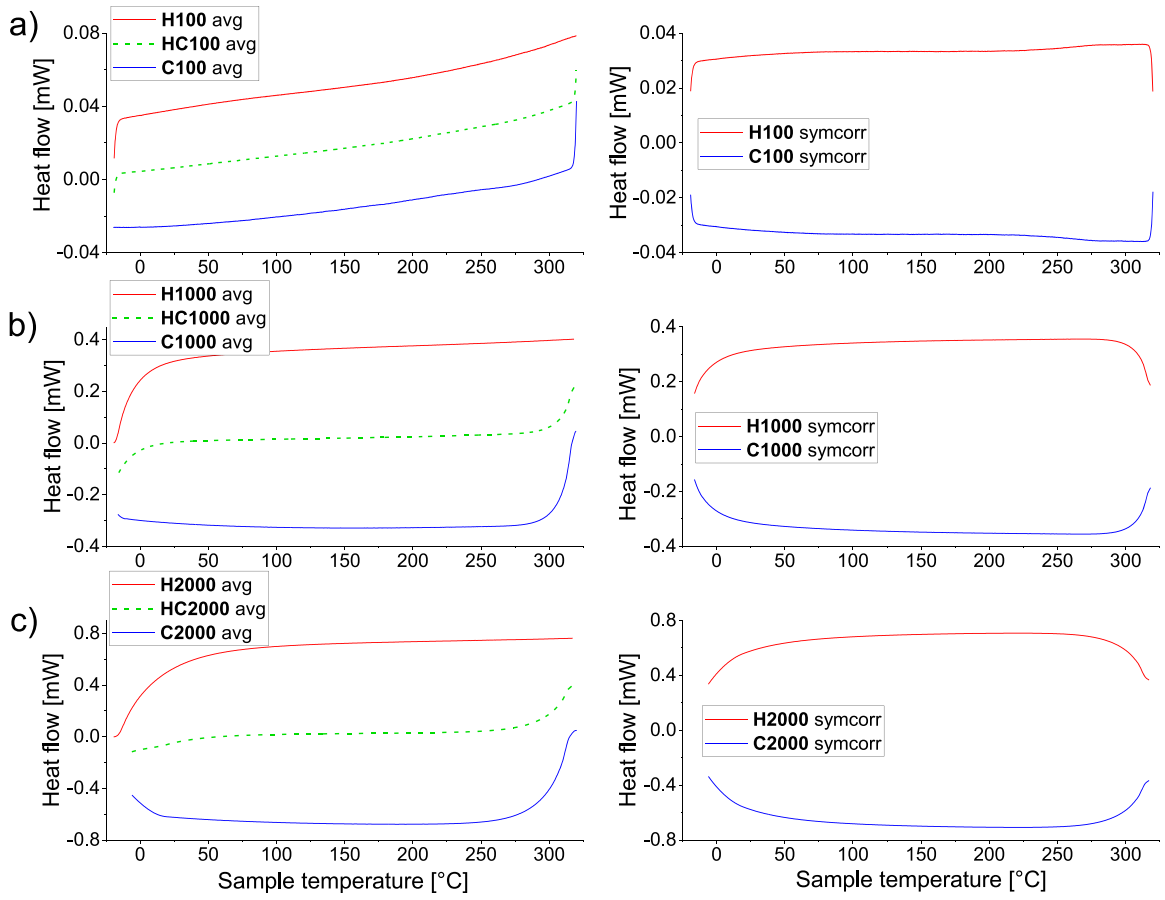

Fig. 5. Symmetry correction method applied to Pb2.6 at a) 100, b) 1000 and c) 2000 K s^{-1}. The left panels show the average of the measured heating and cooling scans, and their average which is the symmetry loss-correction curve (marked as "HCxxx avg" in the legend). The heating scans always show positive heat flow, and cooling scans always negative. The right panels show the result of subtracting the symmetry correction from the measured heat flow. Note that the subtraction yields two identical curves of opposite sign, therefore only one need be evaluated to obtain the corrected c_p curve. Endothermic signal is in the positive y-direction.

3.3. Corrected c_p curves

Having applied the various curve corrections to the measured heat flow, conversion to c_p was then performed by dividing by heating rate and sample mass according to Eq. (5). The results are presented in Fig. 6, using similar scaling to Fig. 2, and show an all-round huge improvement on the uncorrected results. The 100 K s^{-1} curves show the most significant improvement in terms of magnitude, and all the curves show improved linearity after the corrections. Interestingly there is little to distinguish either of the correction methods as superior, though this actually lends reliability to the results. Since both slow-rate and symmetry correction methods aim to determine the real sample heat flow, they should theoretically be identical, and this is more or less what is observed. Furthermore, this consistency between correction methods helps provide an explanation for the overestimation of the c_p, which is noticeable in all of the below figures: as both methods give highly consistent results, the methodology of the corrections seems sound; if the heat flow corrections are not accountable for the overestimation, then it must be introduced in the c_p conversion; if the programmed heating rate is indeed the real heating rate, the only remaining influential parameter is the sample mass. The sample mass was determined from an average melting peak at 100 K s^{-1}, using $\Delta H_{fus}^{Pb} = 4.81\,kJ\,mol^{-1}$ as stated in [2]. Providing this is accurate, the underestimation of the sample mass must be introduced during the measurement and evaluation of the melting peak.

4. Discussion

Beyond the numerical comparisons of c_p for the various samples and scanning rates to the literature, the results gathered present several elements for further discussion in the context of deriving some general optimization rules that can be applied to similar experiments on different systems. The programmed parameters (heating rate and temperate range), the uncertainty of the mass determination, optimum sample mass and the correction method must all be considered to achieve the most accurate c_p result.

The near-identical results from the corrected c_p curves lend credence to both the symmetry and slow-rate correction procedures, even more so than had one been superior in matching the literature expectation. In each measurement instance (given mass and rate), the actual loss function will of course be the same, but the mathematical procedure by which it is calculated differs between the two methods. Whilst there is always a slight overestimation of c_p, the consistence between the methods validates the reliability and practical applicability of both. And, as mentioned before, if the loss correction is not at fault for the overestimation then the determined sample mass used in the c_p conversion (Eq. 5) is most likely the culprit. An improvement on the mass determination might be achieved by evaluating the mass at a variety of heating rates, not just 100 K s^{-1} used here, or perhaps determining the mass through means other than the melting peak.

Since both methods are shown to be a sound choice for predicting

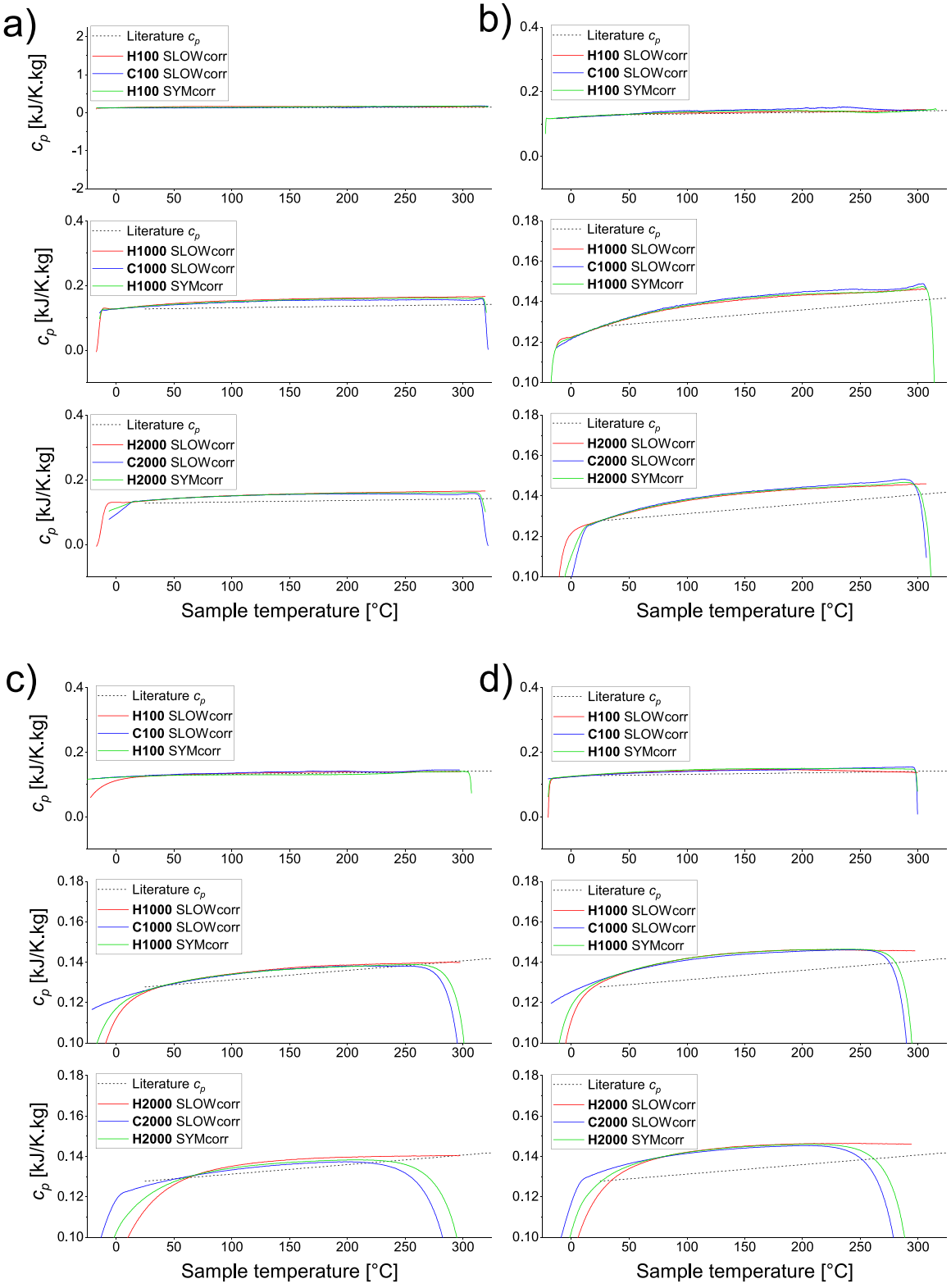

Fig. 6. Specific heat capacity curves calculated after the proposed heat flow correction methods for all masses at all rates. Plots (a), (b), (c) and (d) show masses Pb0.3, Pb1.3, Pb2.6 and Pb5.3 respectively. Rates of 100, 1000 and 2000 K s^{-1} are shown successively in each three plot group. The dotted literature line is produced from [6]. Scaling of each plot matches that of the raw data specific heat curves in Fig. 2. Both slow-rate and symmetry corrections yield very consistent results and show enormous improvement on calculated c_p in the absence of corrections. Best results are observed for mass Pb2.6, though in all cases better linearity is achieved. At higher masses and rates, thermal lag reduces the effective range of results to approximately 50–200 °C.

c_p, when seeking to study a different system either correction procedure could be implemented; however, since the symmetry correction does not require slow-rate measurements, it is less time consuming and is likely preferred for most systems. However, in case of transformations, the slow-rate determination of the baseline may be more appropriate.

Fig. 7 shows the calculated c_p values at 150 °C for the four masses at

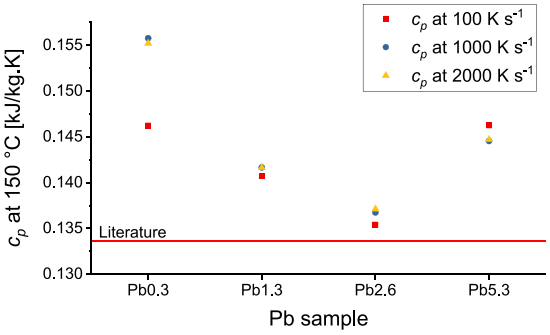

Fig. 7. Sample mass versus c_p at 150 °C for the four samples at 100, 1000 and 2000 K s^{-1} compared to [6]. Each point is an average of the three results from the symmetry and slow-rate corrections on heating and cooling from Fig. 6. The sample Pb2.6 achieves the best results, while high and low masses show higher divergence from the literature value of c_p.

each rate, and allows comparison between the various measurement parameters. Each point in Fig. 7 corresponds to an individual mass and rate, and is the average of the three c_p values produced from the symmetry and slow-rate corrections. Since the two methods give largely similar values in each case, and the c_p curves are all stable and consistent at this temperature, it is appropriate to compare their averages in this manner. One thing is abundantly clear from this diagram: sample mass has a profound effect on the accuracy of the end result. Sample Pb2.6 produces good results, however at higher and lower mass, divergence from the literature value becomes significant. The divergence at low mass (Pb0.3) likely originates from its low heat flow and high signal to noise ratio. This exaggerates the inconsistencies and impact of baseline effects in the signal, and therefore interferes with accurate enthalpy determination for the melting peak. Note that divergence at high mass is only expressed by one point in Fig. 7 and less clear. A probable factor in the accuracy reduction may be the impact of thermal lag and temperature gradients within the sample, which become increasingly exaggerated at higher mass. Whilst the Pb system studied showed 2.56 µg to be close to optimum mass, other metallic systems may differ. The sample's physical size could be part of the reason for Pb2.6's suitability, in which case other systems would differ according to their density. Furthermore, experiments using the new UFH 1 high temperature sensors would certainly exhibit different optimum mass conditions, and a variety of samples would need investigation to determine the most suitable mass.

The second conclusion that can be drawn from Fig. 7 concerns heating rate. In each case, 100 K s^{-1} is seen to be the least consistent. Whilst these inconsistencies are not so significant for Pb1.3, 2.6 and 5.3, for the lowest mass Pb0.3 a large separation of this result is seen compared to those at higher rate. This separation is likely also caused by the small magnitude of the heat flow of the sample compared to the sensor baseline and the worse signal to noise ratio. For c_p measurement of small sample masses (e.g. thin films [25]), it would be best to avoid low heating rates and employ the symmetry correction, along with a very careful determination of the sample mass. So, while a higher sample signal can be achieved at higher heating rate, this also increases the impact of thermal lag in the system and exaggerates the aforementioned stabilization effects. A rate of 1000 K s^{-1} appears a good compromise between these factors for the UFS1 sensors. To compensate for the impact of these stabilization effects on the range of useful results, the temperature range of the measurement can be increased. The possible temperature range is limited however by the chip sensor's operational range, and the melting point of the sample. It is of course possible to heat through and beyond the melting point, or even collect data on the liquid sample, though this may reduce consistency in the system. Also, the solidification peaks can appear over a broad temperature range, and so reduce the effective result range in that manner.

5. Conclusions

In summary, FDSC can be efficiently used to measure specific heat capacity when appropriate heat loss corrections and measurement parameters are applied:

- Both the symmetry and slow-rate correction methods of the heat loss give similar results. Such corrections are in particular important at low sample masses and rates.
- The sample mass shows a stronger influence on the determined c_p-value, than the used heating rate. Intermediate sample masses (2.6 µg for Pb) show the best correlation with literature values for c_p.
- Slight, but consistent overestimation of c_p suggests a small inaccuracy in mass determination.

In the study pure Pb was used, but the applied strategy can serve as a guideline for determining c_p in any other system.

Acknowledgments

This project has received funding from the European Research Council (ERC) under the European Union's Horizon 2020 research and innovation program (grant No. 757961). The authors thank also F. Spieckermann and A. Minotto (Montanuniversitaet Leoben) for fruitful discussions and assistance with the FDSC.

References

[1] S.A. Adamovsky, A.A. Minakov, C. Schick, Scanning microcalorimetry at high cooling rate, Thermochim. Acta 403 (2003) 55–63.
[2] A.A. Minakov1, D.A. Mordvintsev, C. Schick, Melting and reorganization of poly (ethylene terephthalate) on fast heating (1000 K/s), Polymer 45 (2004) 3755–3763.
[3] E. Zhuravlev, C. Schick, Fast scanning power compensated differential scanning nano-calorimeter: 1. The device, Thermochim. Acta 505 (2010) 1–13.
[4] E. Zhuravlev, V. Madhavi, A. Lustiger, R. Androsch, C. Schick, Crystallization of polyethylene at large undercooling, ACS Macro Lett. 5 (2016) 365–370.
[5] E. Tarani, D.G. Papageorgiou, C. Valles, A. Wurm, Z. Terzopoulou, D.N. Bikiaris, C. Schick, K. Chrissafis, G. Vourlias, Insights into crystallization and melting of high density polyethylene/graphene nanocomposites studied by fast scanning calorimetry, Polym. Test. 67 (2018) 349–358.
[6] W.F. Gale, T.C. Totemeir (Eds.), Smithell's Metals Reference Book (8th Edition), Elsevier Inc., Burlington, 2004.
[7] C. Schick, V.B.F. Mathot (Eds.), Fast Scanning Calorimetry, Springer, 2016, , https://doi.org/10.1007/978-3-319-31329-0.
[8] E. Zhuravlev, C. Schick, Fast scanning power compensated differential scanning nano-calorimeter: 2. Heat capacity analysis, Thermochim. Acta 505 (2010) 14–21.
[9] J.E.K. Schawe, Influence of processing conditions on polymer crystallization measured by fast scanning DSC, J. Thermal. Anal. Calorim. 116 (2014) 1165–1173.
[10] S. Pogatscher, D. Leutenegger, A. Hagmann, P.J. Uggowitzer, J.F. Löffler, Characterization of bulk metallic glasses via fast differential scanning calorimetry, Thermochim. Acta 590 (2014) 84–90.
[11] J.E.K. Schawe, S. Pogatscher, Material characterization by fast scanning calorimetry: practice and applications, in: C. Schick, V.B.F. Mathot (Eds.), Fast Scanning Calorimetry, Springer, 2016, pp. 3–80, , https://doi.org/10.1007/978-3-319-31329-0_1.
[12] P. Cebe, B.P. Partlow, D.L. Kaplan, A. Wurm, E. Zhuravlev, C. Schick, Using flash DSC for determining the liquid state heat capacity of silk fibroin, Thermochim. Acta 615 (2015) 8–14.
[13] P. Cebe, D. Thomas, J. Merfeld, B.P. Partlow, D.L. Kaplan, R.G. Alamo, A. Wurm, E. Zhuravlev, C. Schick, Heat of fusion of polymer crystals by fast scanning calorimetry, Polymer 126 (2017) 240–247.
[14] D. Thomas, E. Zhuravlev, A. Wurm, C. Schick, P. Cebe, Fundamental thermal properties of polyvinyl alcohol by fast scanning calorimetry, Polymer 137 (2018) 145–155.
[15] J. Orava, A.L. Greer, B. Gholipour, D.W. Hewak, C.E. Smith, Characterization of supercooled liquid $Ge_2Sb_2Te_5$ and its crystallization by ultrafast-heating calorimetry, Nat. Mater. 11 (2012) 279–283.
[16] J.Q. Wang, N. Chen, P. Liu, Z. Wang, D.V. Louzguine-Luzgin, M.W. Chen, J.H. Perepezko, The ultrastable kinetic behavior of an Au-based nanoglass, Acta Mater. 79 (2014) 30–36.

[17] S. Pogatscher, P.J. Uggowitzer, J.F. Löffler, In-situ probing of metallic glass formation and crystallization upon heating and cooling via fast differential scanning calorimetry, App. Phys. Lett. 104 (2014) 251908.
[18] S. Pogatscher, D. Leutenegger, J.E.K. Schawe, P.J. Uggowitzer, J.F. Löffler, Solid-solid phase transitions via melting in metals, Nat. Commun. 7 (2016) 11113.
[19] B. Chen, J. Momand, P.A. Vermeulen, B.J. Kooi, Crystallization kinetics of supercooled liquid Ge – Sb based on ultrafast calorimetry, Cryst. Growth Des. 16 (2016) 242–248.
[20] P.A. Vermeulen, J. Calon, G.H. ten Brink, B.J. Kooi, Combining ultrafast calorimetry and Electron microscopy: reversible phase transformations in SeTeAs alloys, Cryst. Growth Des. 18 (2018) 3668–3673.
[21] J.H. Perepezko, T.W. Glendenning, J.-Q. Wang, Nanocalorimetry measurements of metastable states, Thermochim. Acta 603 (2015) 24–28.
[22] H. Weber, J. Orava, I. Kaban, J. Pries, A.L. Greer, Correlating ultrafast calorimetry, viscosity, and structural measurements in liquid GeTe and Ge15Te85, Phys. Rev. Mat. 2 (2018) 093405.
[23] G. Kurtuldu, K.F. Shamlaye, J.F. Löffler, Metastable quasicrystal-induced nucleation in a bulk glass-forming liquid, PNAS 115 (2018) 6123–6128.
[24] G.W.H. Höhne, W. Hemminger, H.-J. Flammersheim, Differential Scanning Calorimetry: An Introduction for Practitioners, Springer, 2003.
[25] J. Yu, Z. Tang, F. Zhang, H. Ding, Z. Huang, Heat Capacity of Copper Thin Films Measured by Micropulse Calorimeter, ICNMM 2008, Darmstadt, Germany, June 23-25 (2008).